Leaf phenology as one important driver of seasonal changes in isoprene emission in central Amazonia

Eliane G. Alves[1], *Julio Tóta*[2], *Andrew Turnipseed*[3], *Alex B. Guenther*[4], *José Oscar W. Vega Bustillos*[5], *Raoni A. Santana*[2], *Glauber G. Cirino*[6], *Julia V. Tavares*[1], *Aline P. Lopes*[1], *Bruce W. Nelson*[1], *Rodrigo A. de Souza*[7], *Dasa Gu*[4], *Trissevgeni Stavrakou*[8], *David K. Adams*[9], *Jin Wu*[10], *Scott Saleska*[11], *Antonio O. Manzi*[12].

[1] Department of Environmental Dynamics, National Institute for Amazonian Research (INPA), Av. André Araújo 2936, CEP 69067-375, Manaus-AM, Brazil.

[2] Institute of Engineering and Geoscience, Federal University of West Para (UFOPA), Rua Vera Paz s/n, CEP 68035-110, Santarem-PA, Brazil.

[3] 2B Technologies, Inc., 2100 Central Ave., Boulder, CO 80301, U.S.A.

[4] Department of Earth System Science, University of California, Irvine, CA 92697, USA.

[5] Chemistry and Environment Center, National Institute for Energy and Nuclear Research (IPEN), Av. Lineu Prestes 2242, CEP 05508-000, São Paulo-SP, Brazil.

[6] Department of Meteorology, Geosciences Institute, Federal University of Para, Belém, PA 66075-110, Brazil

[7] Meteorology Department, State University of Amazonas (UEA), Av. Darcy Vargas 1200, CEP 69050-020, Manaus-AM, Brazil.

[8] Royal Belgian Institute for Space Aeronomy, Avenue Circulaire 3, 1180, Brussels, Belgium.

[9] Centro de Ciencias de la Atmósfera, Universidad Nacional Autónoma de México, Av. Universidad 3000, 04510, Mexico city, Federal District, Mexico.

[10] Department of Environmental and Climate Sciences, Brookhaven National Laboratory, Upton, NY 11973, USA.

[11] Ecology and Evolutionary Biology Department, University of Arizona, Cherry Avenue and University Boulevard, Tucson, AZ 85721, USA.

[12] National Institute for Spatial Research, Center of Weather Forecasting and Climate Studies, Rod. Presidente Dutra, km 40, Cachoeira Paulista-SP, Brazil.

corresponding author: +55 92 3643 3238; elianegomes.alves@gmail.com

Abstract

Isoprene fluxes vary seasonally with changes in environmental factors (e.g., solar radiation and temperature) and biological factors (e.g., leaf phenology). However, our understanding of seasonal patterns of isoprene fluxes and associated mechanistic controls are still limited, especially in Amazonian evergreen forests. In this paper, we aim to connect intensive, field-based measurements of canopy isoprene flux over a central Amazonian evergreen forest site, with meteorological observations and with tower mounted camera leaf phenology to improve understanding of patterns and causes of isoprene flux seasonality. Our results demonstrate that the highest isoprene emissions are observed during the dry and dry-to-wet transition seasons, whereas the lowest emissions were found during the wet-to-dry transition season. Our results also indicate that light and temperature can not totally explain isoprene flux seasonality. Instead, the camera-derived leaf area index (LAI) of recently mature leaf-age class (e.g. leaf ages of 3-5 months) exhibits the highest correlation with observed isoprene flux seasonality (R^2=0.59, p<0.05). Attempting to better represent leaf phenology in the Model of Emissions of

Gases and Aerosols from Nature (MEGAN 2.1), we improved the leaf age algorithm utilizing results from the camera-derived leaf phenology that provided LAI categorized in three different leaf ages. The model results show that the observations of age-dependent isoprene emission capacity, in conjunction with camera-derived leaf age demography, significantly improved simulations in terms of seasonal variations of isoprene fluxes (R^2=0.52, p<0.05). This study highlights the importance of accounting for differences in isoprene emission capacity across canopy leaf age classes and of identifying forest adaptive mechanisms that underlie seasonal variation of isoprene emissions in Amazonia.

1. Introduction

Isoprene is considered the dominant contribution to Biogenic Volatile Organic Compound (BVOC) emission from many landscapes and represents the largest input to total global BVOC emission, which has the magnitude of 400-600 Tg C y^{-1} (see Table 1 of Arneth et al., 2008). This compound regulates large-scale biogeochemical cycles. For example, once in the atmosphere, isoprene has implications for chemical and physical processes due to its reactivity, influences on the atmospheric oxidative capacity, as well as its potential to form secondary organic aerosols (Claeys et al., 2004), which interact with solar radiation and act as effective cloud condensation nuclei. Moreover, isoprene emissions could play an important role in the carbon balance, because it has the largest contribution to total BVOCs, which are regarded as highly significant for net ecosystem productivity, with their losses comparable to the magnitude of net biome productivity (Kesselmeier et al., 2002); and carbon dioxide is believed to be the fate of almost half of the carbon released in the form of BVOCs (Goldstein and Galbally, 2007).

69 Tropical forests are the largest source of isoprene for the atmosphere, contributing
70 almost half of the estimated global annual isoprene emission, according to Model of
71 Emissions of Gases and Aerosols from Nature (MEGAN) estimates (Guenther et al.,
72 2006). Given that the Amazon basin is the largest territorial contribution to global
73 tropical forests, this ecosystem is thought to be one of the most important sources of
74 isoprene for the global atmosphere.

75 Recently, remotely sensed observations from multiple years have revealed
76 seasonal changes in isoprene emission over the Amazonian rainforest (Barkley et al.,
77 2008, 2009, 2013, Bauwens et al., 2016). Apart from these remotely sensed data, only a
78 few studies based on *in situ* data exist (Alves et al., 2016; Andreae et al., 2002;
79 Kesselmeier et al., 2002; Kuhn et al., 2004b; Yáñez-Serrano et al., 2015). Some of these
80 *in situ* studies indicate that environmental factors such as solar radiation and temperature
81 are primary drivers of isoprene emissions (Andreae et al., 2002; Kesselmeier et al., 2002;
82 Kuhn et al., 2004b; Yáñez-Serrano et al., 2015).

83 However, besides long-term seasonal variation in light and temperature, other
84 biological factors might act on seasonal changes of isoprene emission, as in the case of
85 canopy phenology. Previous studies with temperate species have shown that isoprene
86 emission capacity is affected by leaf age and ontogeny (Kuzma and Fall, 1993;
87 Mayrhofer et al., 2005; Monson et al., 1994), because: (1) isoprene synthase and other
88 enzymes of isoprene synthesis pathway (MEP pathway) depends on the leaf ontogeny -
89 isoprene synthase activity is low or absent in very young leaves, increases gradually until
90 full leaf maturation, and decreases with leaf senescence (Schnitzler et al., 1997); (2) for
91 species with non-senescent leaves, or with a life-span of more than one year, foliage

92 shading and time-dependent changes of physiological activity of leaves could decrease
93 isoprene emission capacity (Niinemets et al., 2004, 2010); and (3) leaf structure varies
94 with leaf ontogenetic stage, indicating that seasonal isoprene emission capacity is also
95 affected by seasonal structural changes in leaves (Niinemets et al., 2004, 2010).

96 Leaf phenology, with notable seasonal changes in the Amazonian rainforest, was
97 just recently discovered (Huete et al., 2006; Lopes et al., 2016; Myneni et al., 2007;
98 Saleska et al., 2016; Wagner et al., 2017), and there is still some debate about it (e.g.
99 Morton et al., 2014; Samanta et al., 2010). Given that for many years seasonal changes
100 and leaf phenology were thought to be unimportant for tropical forests, assumed to be in
101 an evergreen condition state, led the scientific modeling community to assume that leaf
102 phenology has little affect on forest and atmosphere gas exchanges in the tropics.
103 However, after remote sensing studies showed seasonal biomass changes (Myneni et al.,
104 2007) and seasonal changes in isoprene emissions (Barkley et al., 2009, 2013), models
105 were improved in order to better represent seasonal biomass changes and leaf age in
106 tropical forests.

107 MEGAN already uses variations in LAI to parameterize changes in leaf age to
108 stimulate changes in the emission activity factor of isoprene emission (Guenther et al.,
109 2012). However, because leaf phenology in tropical forests is not as notable as in
110 temperate forests, some insights on how changes in leaf age over the year may affect
111 seasonal isoprene emissions are still missing, and there is a lack of representation of this
112 process in models. Here, our goal is to demonstrate that leaf phenology affects seasonal
113 changes of isoprene emission and this is, in fact, new information for tropical forests.

In this study, we present observations of seasonal variation of isoprene flux, solar radiation, air temperature and canopy phenology from a primary rainforest site in central Amazonia. The questions addressed are: (i) how much can seasonal isoprene fluxes be explained by variations in solar radiation, temperature and leaf phenology, and (ii) how can a consideration of leaf phenology observed in the field help to improve model estimates of seasonal isoprene emissions. To this end, we correlate ground-based isoprene flux measurements with environmental factors (light and temperature) and a biological factor (leaf phenology). We compare seasonal ground-based isoprene flux measurements to OMI satellite-derived isoprene flux. Lastly, we perform two simulations with the MEGAN 2.1 to estimate isoprene fluxes: (1) with standard emission algorithms and (2) with a modification in the leaf age algorithm derived from observed leaf phenology.

2. Material and methods

2.1. Site Description - Cuieiras Biological Reserve – K34 site

Isoprene fluxes were measured at the 53 m K34 tower (2°36' 32.6" S, 60° 12' 33.4" W) on the Cuieiras Biological Reserve plateau, a primary rainforest reserve approximately 60 km northwest of Manaus in Amazonas state, Brazil (Fig. 1). The K34 tower has been widely utilized for the past 15 years for a range of meteorological studies, including energy and trace gas fluxes (de Araújo et al., 2010; Artaxo et al., 2013; Tóta et al., 2012) and also tropospheric variables such as precipitable water vapor (Adams et al., 2011, 2015). This reserve has an area of about 230 km² and is managed by the National Institute for Amazonian Research (INPA). The site has a maximum altitude of 120 m and

the topography is characterized by 31% plateau, 26% slope and 43% valley (Rennó et al., 2008). The vegetation in this area is considered mature, *terra firme* rainforest, and with typical canopy height of 30 m with variation (20-45 m) throughout the reserve. More details about soils and vegetation at this site are provided in Alves et al. (2016). Annual precipitation is about 2500 mm and is dominated by deep atmospheric convection and associated stratiform precipitation, December to May being the wet season and August to September the dry season, when the monthly cumulative precipitation is less than 100 mm (Adams et al., 2013; Machado et al., 2004). Average air temperature ranges between 24 °C (in April) and 27 °C (in September) (Alves et al., 2016).

2.2. Isoprene flux – Relaxed Eddy Accumulation system (REA)

Isoprene flux measurements were conducted during intensive campaigns of five to six days, between the 20^{th} and 30^{th} of each month, during daytime (9:00-16:30, local time), from June 2013 to December 2013 at the K34 tower. The REA system utilized for the isoprene flux measurements was developed by the National Center for Atmospheric Research (NCAR) NCAR/BEACHON REA Cassette Sampler), and has two basic components: 1) the main REA box containing the adsorbent cartridges (stainless steel tubes filled with Tenax TA and Carbograph 5 TD adsorbents) for up/down/neutral reservoirs, microcontroller, battery, selection valves, and mass flow controller (200 ml min^{-1}) (MKS Instruments Inc., Model M100B01852CS1BV); and (2) a Sonic Anemometer (RM Young, Model 81000VRE) for high-rate wind velocity measurements (10 Hz). This REA system was installed at a height of 48 m on the K34 tower (approximately 20 m above the mean canopy height).

160 The technique segregated the sample flow according to sonic anemometer-derived
161 vertical wind velocity over the flux-averaging period (30 min). Isoprene fluxes (*F*) from
162 the REA system over this period were estimated from:

163 $$F = \overline{w'c'} = b\sigma_w(\overline{c_{up}} - \overline{c_{down}}) \quad (1)$$

164 where *b* is an empirical proportionality coefficient (described below), σ_w is the standard
165 deviation of *w*, and $\overline{c_{up}}$ and $\overline{c_{down}}$ are isoprene concentration averages in the up and
166 down reservoirs, respectively (Bowling et al., 1998). The *b*-coefficient was calculated
167 from the sonic temperature and heat flux by re-arranging the same equation, assuming
168 scalar similarity (Monin-Obukhov Similarity Theory):

169 $$b = \frac{\overline{w'T'}}{\sigma_w(T_{up} - T_{down})} \quad (2)$$

170 The REA sampler was operated with a "deadband" - a range of small w' values,
171 centered on $\overline{w}$, over which the air was sampled through the "neutral" line. The deadband
172 used was $\pm 0.6\sigma_w$. The use of a deadband was advisable, because this increased the
173 differences in the measured concentrations ($\overline{c_{up}} - \overline{c_{down}}$) by sampling only larger eddies
174 (with larger concentration fluctuations) into the up/down reservoirs, reducing the
175 precision required for the analytical measurements. The *b*-coefficient was also computed
176 (from Eq. (2)) using the same deadband. For this study, the *b*-coefficient was calculated
177 for every 30 min. flux-sampling period. The *b*-coefficient averaged 0.40 ± 0.06 and the
178 flux measurements were filtered for *b*-coefficients in the range of 0.3 to 0.6.

179 The air sampling was carried out with two tubing lines for up (+w') and down (-
180 w') and one tubing line for neutral sampling air ($\pm 0.6\sigma_w$ - deadband), each consisting of
181 approximately 1.5 m long tubes (polytetrafluoroethylene, PTFE) positioned such that
182 they sampled air as close to the sonic anemometer as possible. Each inlet valve at the

183 main REA box prevented air from entering the inactive tube (up- in the case of down
184 sampling (-w') and down - in the case of up sampling (+w'), and both up and down in the
185 case of deadband), which otherwise would compromise the concentration differences
186 between up and down reservoirs and, consequently, the flux calculation.

187 The microcontroller recorded the sonic anemometer data and triggered the
188 segregation valves based on this data. The REA technique requires two initial data points
189 prior to each flux averaging period to be able to segregate the sample flow: (1) a mean
190 vertical wind velocity, $\overline{w}$ and (2) σ_w. The $\overline{w}$ determined the direction of the instantaneous
191 vertical wind velocity ($w' = w(t) - \overline{w}$) and σ_w was required to calculate the deadband
192 threshold. Both the value of $\overline{w}$ and σ_w were based on the values obtained from the last
193 flux-averaging period (30 min). The microcontroller stored all the necessary wind and
194 temperature information to compute all the parameters required in the equations (1) and
195 (2). More details on errors and uncertainties of the REA technique are found in section 1
196 (Supplementary Information).

197
198 **2.3. Isoprene concentrations**

199 The isoprene accumulated in the adsorbent cartridges was determined from
200 laboratory analysis. The tube samples were analyzed with a thermal desorption system
201 (TD) (Markes International, UK) interfaced with a gas chromatograph/flame ionization
202 detector (GC-FID) (19091J-413 series, Agilent Technologies, USA). After loading a tube
203 in the ULTRA Automatic Sampler (Model Ultra1, Markes International, UK), which was
204 connected to the thermal desorption system, the collected samples were dried by purging
205 for 5 minutes with 50 sccm of ultra-high purity helium (all flow vented out of the split
206 vent) before being transferred (300ºC for 10 min with 50 sccm of ultra-pure nitrogen) to

207 the thermal desorption cold trap held at -10 ºC (Unity Series1, Markes International, UK).
208 During GC injection, the trap was heated to 300°C for 3 min while back flushing with
209 carrier gas (helium) at a flow rate of 6.0 sccm directed into the column (Agilent HP-5 5%
210 Phenyl Methyl Siloxane Capillary 30.0 m X 320 µm X 0.25 µm). The oven ramp
211 temperature was programmed with an initial hold of 6 min at 27 °C followed by an
212 increase to 85 °C at 6 °C min^{-1} followed by a hold at 200 °C for 6 min. The identification
213 of isoprene from samples was confirmed by comparison of retention time with a solution
214 of an authentic isoprene liquid standard in methanol (10 µg/ml in methanol, Sigma-
215 Aldrich, USA). The GC-FID was calibrated to isoprene by injecting 0.0, 23, 35, and 47
216 nL of the gas standard into separate tubes. The gas standard is 99.9% of 500 ppb of
217 isoprene in nitrogen (Apel & Riemer Environmental Inc., USA) and was injected into
218 separate tubes at 11 ml min^{-1}. The calibration curve (0.0, 23, 35, and 47 nL) was made
219 thrice before the analysis of the sample tubes of each campaign, with a mean correlation
220 coefficient equal to R^2=0.98. In addition, two standard tubes (with 35 nL of isoprene)
221 were run at every 20 sample tubes to check the system sensitivity. The limit of detection
222 of isoprene was equal to 48.4 ppt. All tube samples were analyzed as described above
223 with the exception of tube samples from June 2013 and July 2013. These were analyzed
224 in a TD/GC-MS-FID system from the Atmospheric Chemistry Division, NCAR (see
225 section 1 of supplementary information for more details).

226 Isoprene concentration was determined using the sample volume that was passed
227 through each tube. This volume was measured by integration of the mass flow meter
228 signal and stored within the REA data file. While sampling, the concentration found in
229 the blank tubes connected to the cartridge cassette in the REA box, but without flow, was

230 subtracted from the sample tube concentrations. The resulting concentration was used to
231 calculate isoprene flux (Eq. (1)) in mg m^{-2} h^{-1}.
232
233 **2.4. Tower-camera derived leaf phenology and demography**
234 Upper canopy leaf phenology was monitored with Stardot RGB imaging system
235 (model Netcam XL 3MP) installed at 51 m height on the K34 tower (Lopes et al., 2016;
236 Nelson et al., 2014; Wu et al., 2016). The system used the native CMOS resolution of
237 1024 x 768 pixels and a varifocal lens (Stardot reference LEN-MV4510CS), adjusted to
238 about 66^{o} HFOV. The camera was set to automatic exposure and did not apply automatic
239 color balance. The view was fixed with south azimuth toward a forested plateau area,
240 monitoring the same crowns over time and excluding the sky, so that auto-exposure was
241 based only on the forest. This system was locally controlled by a Compulab
242 microcomputer (model Fit-PC2i), which stored the images *in situ*. Images were
243 automatically logged every two minutes from 09:00h to 12:30h, local time. Only images
244 acquired near local noon and under overcast sky (having even diffuse illumination) were
245 analyzed. Images were selected at six-day intervals. The camera monitored upper crown
246 surfaces of 53 living trees over 24 months (1 December 2011 to 31 November 2013).
247 We used a camera-based tree inventory approach to monitor leaf phenology at this
248 forest site (Lopes et al., 2016; Nelson et al., 2014; Wu et al., 2016). Specifically, we
249 visually tracked the temporal trajectory of each tree crown, and assigned them into one of
250 three classes: “leaf flushing” (crowns which showed a large abrupt greening), “leaf
251 abscising” (crowns which showed large abrupt greying, which is the color of bare upper
252 canopy branches) or “no change”. We then aggregated our census to the monthly scale to

253 derive the monthly-average percentages of trees with new leaf flushing and with old leaf
254 abscission. The percentage of tree crowns with green leaves (1 – the percentage of tree
255 crowns with leaf abscission) is termed as “green crown fraction” (Wu et al., 2016). We
256 obtained a camera-based canopy LAI by applying the same linear relationship between
257 ground-measured LAI and camera-derived green crown fraction, fitted at another central
258 Amazon evergreen forest, the Tapajós K67 tower site (Wu et al., 2016). As the fraction of
259 all crowns classified to the abscised state has been shown to be linearly and inversely
260 proportional to total canopy LAI at seasonal timescales (Wu et al., 2016), it was used at
261 K34 to provide a camera-based estimate of temporal variation in canopy LAI.
262 We also estimated the monthly canopy leaf demography by tracking the post-leaf-
263 flush age of each crown's leaf cohort and sorting them into three leaf age classes
264 throughout the year (young: <=2 months; mature: 3-5 months; and old: >=6 months)
265 (Nelson et al., 2014; Wu et al., 2016). By multiplying camera-derived total LAI by the
266 camera-derived fraction of crowns in a given age class, LAIs were derived for the three
267 leaf age classes: young leaf LAI, mature leaf LAI, and old leaf LAI.
268
269 **2.5. Modeled isoprene flux estimates - MEGAN 2.1**
270 Isoprene fluxes measured by REA (K34 site) were compared with those estimated
271 by MEGAN 2.1. Isoprene emissions estimated by MEGAN 2.1 account for the main
272 processes driving variations in emissions (Guenther et al., 2012). The isoprene flux
273 activity factor for isoprene (γ_i) is proportional to emission response to light (γ_P),
274 temperature (γ_T), leaf age (γ_A), soil moisture (γ_{SM}), leaf area index (LAI) and CO_2
275 inhibition (γ_{CO2}) according to Eq. (3):

$$\gamma_i = C_{CE} LAI \gamma_P \gamma_T \gamma_A \gamma_{SM} \gamma_{CO_2} \quad (3)$$

where C_{CE} is the canopy environment coefficient. For this study, the canopy environment model of Guenther et al. (2006) was used with a C_{CE} of 0.57. MEGAN 2.1 was run accounting for variations in light, temperature, and LAI. Based on changes in LAI, the model estimated foliage leaf age. Both CO_2 inhibition and soil moisture activity factors were set equal to a constant of 1, assuming these parameters do not vary. In terms of soil moisture, no seasonal variation in the model was assumed because a previous study showed that during the dry season there is only a small reduction (~10 %) in soil moisture compared to the wet season (Cuartas et al., 2012); and this reduction does not induce water stress to this forest region (Wagner et al., 2017). Moreover, based on the dataset of soil moisture shown from 2002 to 2006 (Cuartas et al., 2012), the soil moisture always exceeds the threshold for the isoprene drought response in MEGAN 2.1 (Guenther et al., 2012), which means that MEGAN would predict that there are no variations in isoprene emissions due to these observed changes in soil moisture. Details on model settings are found in Guenther et al. (2012).

Photosynthetic photon flux density (PPFD) and air temperature inputs for all model simulations were obtained from measurements at the K34 tower. PPFD and air temperature measured at tower top, every 30 minutes, were hourly averaged. Data gaps during certain months occurred in 2013, but at least 15 days of hourly average PPFD and air temperature were obtained for model input. LAI inputs were acquired from the Moderate Resolution Imaging Spectroradiometer (MODIS) satellite observations for the same period of the isoprene flux measurements. The level-4 LAI product is composited every 8 days at 1-km resolution on a sinusoidal grid (MCD15A2H) (Myneni, 2015).

299 Additionally, by comparison with the standard MEGAN 2.1 model that uses MODIS-
300 derived LAI variation, here we also used LAI fractionated into different leaf ages, which
301 were obtained from tower camera observations (as described in the section above). The
302 number of data inputs to the MEGAN simulations is summarized in table 1.
303
304 **2.6. Satellite-derived isoprene flux estimates**
305 Top-down isoprene emission estimates over the 0.5 degree region around the tower were
306 obtained by applying a grid-based source inversion scheme (Stavrakou et al., 2009, 2015)
307 constrained by satellite formaldehyde (HCHO) columns, measured in the UV-visible by
308 the Ozone Monitoring Instrument (OMI) onboard the Aura satellite launched in 2004.
309 HCHO is a high yield intermediate product in the isoprene degradation process
310 (Stavrakou et al., 2014). The source inversion was performed using the global chemistry-
311 transport model IMAGESv2 (Intermediate Model of Annual and Global Evolution of
312 Species) at a resolution of 2º × 2.5º and 40 vertical levels from the surface to the lower
313 stratosphere (Stavrakou et al., 2014, 2015). The a priori isoprene emission inventory was
314 taken from MEGAN-MOHYCAN (Stavrakou et al., 2014, http://emissions.aeronomie.be,
315 Bauwens et al. 2017). Given that the OMI overpass time is in the early afternoon (13:30,
316 local time), and the mostly delayed production of formaldehyde from isoprene oxidation,
317 the top-down emission estimates rely on the ability of MEGAN to simulate the diurnal
318 isoprene emission cycle and on the parameterization of chemical and physical processes
319 affecting isoprene and its degradation products in IMAGESv2. For this study, we use
320 daily (24 hours), mean satellite-derived isoprene emissions derived from January 2005 to

December 2013. More details can be found in Stavrakou et al. (2009, 2015) and Bauwens et al. (2016).

3. Results

The experimental site of this study showed seasonal variation in air temperature and in photosynthetic active radiation (PAR) (Fig. 2a,b) that was comparable to the seasonality presented by the OMI satellite-derived isoprene fluxes for the K34 site domain (Fig. 2c). The interannual variation in the seasonality of these environmental factors, air temperature and PAR, was correlated to the one presented by the satellite-derived isoprene fluxes, with the highest correlation found between satellite-derived isoprene fluxes and air temperature. Isoprene fluxes and PAR - R^2 ranged from 0.34 to 0.83 $p<0.05$; isoprene fluxes and air temperature - R^2 ranged from 0.61 to 0.91, $p<0.01$, from 2005 to 2013. Maxima and minima of PAR, air temperature, and satellite-derived isoprene fluxes were observed during the dry and the dry-to-wet transition seasons, and the wet and the wet-to-dry transition seasons, respectively.

As opposed to the average (2005-2013) flux peaking in September, the 2013 results suggest a maximum in October, and are found to be substantially lower during the 2013 dry season compared to the average of the dry season estimates (reduction of ~31%) (Fig. 2c). The timing of the maximum is not supported by the ground-based observations, peaking in September, but the magnitude of flux estimates in these two months are in good agreement. In the wet-to-dry transition period, the small reduction in satellite-based isoprene fluxes in July 2013, compared to the neighboring months, is corroborated by a similar behavior in the ground-based isoprene fluxes (Fig. 3d). However, the drop in the

observations is much stronger than in the top-down estimates (factor of 3 vs. a 70% difference).

Different from satellite-derived fluxes, ground-based isoprene fluxes measured with the REA system have not shown significant correlation with PAR and air temperature for the year 2013 (Table 2 and Fig. 3). Ground-based isoprene fluxes also showed the maximum emission during the dry season (September), but emissions remained high in the beginning of the wet season (December), which was not observed in the seasonal behavior of PAR and air temperature. When averages of air temperature and PAR measured only during the same days of REA isoprene flux measurements were compared to isoprene fluxes, the correlations coefficients increased, but were still not statically significant (Table 2).

The forest leaf quantity, shown as Leaf Area Index (LAI), varied little over the year when the total LAI was examined. However, when total LAI was fractionated into three different leaf age classes – young LAI (<=2 months), mature LAI (3-5 months), and old LAI (>=6 months), seasonal variation of each age class appears (Fig. 4). To understand how those LAI age fractions are related to the isoprene seasonality, ground-based fluxes of this compound were compared to the LAI age fractions estimated over the entire year (Fig. 4). The highest emissions were observed when the number of trees with mature leaves (mature LAI) was increasing and the number of trees with old leaves (old LAI) was decreasing. Considering seasonal changes in PAR, air temperature, and mature LAI, the latter presented the highest correlation coefficient, explaining 59% of the seasonal isoprene emission variations (Table 2).

366 Isoprene flux simulations carried out with MEGAN 2.1 reveal similarities with the
367 magnitudes observed during several months. But, MEGAN 2.1 did not fully capture the
368 observed seasonal behavior (Fig. 5). Even though the leaf-age algorithm of MEGAN 2.1
369 was parameterized with local leaf phenology observations, giving the highest correlation
370 coefficient with observed fluxes (Table 2), isoprene flux simulations with local
371 CAMERA-LAI inputs showed only a reduction in isoprene flux magnitudes. The
372 seasonal behavior observed was the same as in the estimates from the default MEGAN
373 2.1 with MODIS-LAI inputs. Regressions between averages of observations and
374 MEGAN 2.1 estimates, with CAMERA-LAI and MODIS-LAI inputs, were weak and not
375 statistically significant (Table 2).
376 As a sensitivity test, observations of isoprene emission capacity at different leaf
377 ages of a central Amazonian hyper-dominant tree species, *Eschweilera coriacea* (Alves et
378 al., 2014), were used to parameterize the MEGAN 2.1 leaf age algorithm. Leaf level
379 measurements of isoprene emission capacity are scarce in Amazonia. To the best of the
380 authors' knowledge, Alves et al. (2014) are the only available data of leaf level isoprene
381 emission capacity at different leaf ages of a central Amazonian tree species, which were
382 therefore used for the MEGAN sensitivity test.
383 Further simulations were performed with modifications in the leaf age emission
384 activity factor (EAF), which is dimensionless and is defined as the emission relative to
385 the emission of mature leaves that are, by definition, set equal to one. A new EAF was
386 assigned for each age class, based on observations of emissions of *E. coriacea* (Fig. 6).
387 Leaf age fraction distribution was provided with input of LAI from MODIS (MODIS-
388 LAI) and from LAI-derived field observations (CAMERA-LAI) (Fig. 4). The simulation

389 with the leaf age algorithm parameterized for EAF changes and with MODIS-LAI was
390 similar to the one without changes in the EAF (MEGAN 2.1 default). The simulation
391 with leaf age algorithm parameterized with changes in the EAF and with CAMERA-LAI
392 inputs showed reduced emissions, but a seasonal curve closer to that of isoprene flux
393 observed at K34 (R^2 = 0.52, p<0.05) (Table 2).
394
395 **4. Discussion**
396 This study addressed two main questions with respect to the seasonality of
397 isoprene fluxes in central Amazonia and identified possible limitations in our current
398 understanding related to these questions.
399 **4.1. How much can seasonal isoprene fluxes be explained by variations in solar**
400 **radiation, temperature, and leaf phenology?**
401 Our finding that isoprene emissions are higher during the warmer season is
402 consistent with previous findings that emissions from tropical tree species are light
403 dependent and stimulated by high temperatures (Alves et al., 2014; Harley et al., 2004;
404 Jardine et al., 2014; Kuhn et al., 2002, 2004a, 2004b). Indeed, satellite-derived isoprene
405 fluxes (2005-2013 years) were well correlated to PAR and even more to air temperature
406 for all years. However, high ground-based isoprene emissions were observed until late of
407 dry-to-wet transition season, when mean PAR and air temperature were already
408 decreasing.
409 The reasons why satellite-derived isoprene fluxes are weakly correlated to
410 ground-based isoprene fluxes can be attributed to either the difference in the studied
411 scales (e.g., local effects could have major influences on ground-based isoprene fluxes)

412 and/or the uncertainties associated with the methodologies used to estimate or calculate
413 fluxes. The high correlation between satellite-based fluxes and air temperature or PAR is
414 not unexpected, because higher temperatures and solar radiation fluxes favor isoprene
415 emissions. Note however that the satellite-derived fluxes might also be subject to inherent
416 uncertainties, due to the existence of other HCHO sources, in particular biomass burning
417 (during the dry season) and methane oxidation. Since these latter contributions are
418 favored by high temperature and radiation levels, they could possibly contribute to the
419 high correlation found between satellite-based isoprene and meteorological variables.
420 For the ground-based emission, isoprene fluxes were determined by REA
421 measurements that were carried out for six days per month. Therefore, the low correlation
422 between ground-based isoprene fluxes and air temperature and PAR could partially result
423 from limited qualified data.
424 Another factor correlated to ground-based isoprene fluxes is the leaf phenology
425 (in this study, LAI fractionated into age classes). The ground-based isoprene fluxes
426 correlated better to variation of mature LAI than to other factors (K34 site – R^2=59%,
427 p<0.05), suggesting that the increasing isoprene emissions could partially follow the
428 increasing of mature leaves (Fig. 4). Wu et al. (2016) suggested that leaf demography
429 (canopy leaf age composition) and leaf ontogeny (age-dependent photosynthetic
430 efficiency) are the main reasons for the seasonal variation of the ecosystem
431 photosynthetic capacity in Amazonia. Photosynthesis supplies the carbon to the methyl
432 erythritol phosphate pathway to produce isoprene (Delwiche and Sharkey, 1993; Harley
433 et al., 1999; Lichtenthaler et al., 1997; Loreto and Sharkey, 1993; Rohmer, 2008;
434 Schwender et al., 1997), and isoprene emissions are strongly dependent on leaf

435 ontogenetic stage - due to the developmental patterns of isoprene synthase activity that
436 gradually increases with leaf maturation and decreases with leaf senescence (Alves et al.,
437 2014; Kuzma and Fall, 1993; Mayrhofer et al., 2005; Monson et al., 1994; Niinemets et
438 al., 2004, 2010; Schnitzler et al., 1997). Therefore, seasonal changes in the forest leaf-age
439 fractions may also influence the seasonality of isoprene emissions, suggesting higher
440 emissions in the presence of more mature leaves and during high ecosystem
441 photosynthetic capacity efficiency.

442 Understanding the correlations among light, temperature, leaf phenology (LAI
443 fractionated into age classes), and isoprene is not straightforward. The weak correlation
444 of seasonal changes between isoprene and light and temperature might be due to seasonal
445 changes in the isoprene dependency to environmental factors and biological factors. Light
446 and temperature peaked at the dry season; mature LAI, Gross Primary Productivity (GPP)
447 and photosynthetic capacity peaked at the wet season (Wu et al., 2016); and ground-
448 based isoprene fluxes were high from the end of the dry to the dry-to-wet transition
449 seasons. This might suggest that isoprene emissions are stimulated by light and high
450 temperature during the beginning of the dry season and offset by the lower amount of
451 mature leaves. During the wet season, isoprene emissions could be stimulated by the
452 higher abundance of mature leaves and offset by the lower light availability and lower
453 temperature. But, at the end of the dry and at dry-to-wet transition seasons, there is a
454 combination of increased light and high temperature with a large amount of mature
455 leaves, possibly favoring high isoprene emissions.

456 This is supported by findings of a temperate plant species showing that LAI
457 dependency (changes in leaf age) was the most important factor affecting isoprene

emission capacity, but when LAI decreased, and senescence started at the end of the summer, the isoprene dependency to PAR and air temperature was as high as the period when PAR and air temperature reached their maximum (Brilli et al., 2016). This shows seasonal variation in the strength of dependency to each factor that affects emissions.

As discussed above, separating the effects of changing temperature and light from leaf phenology in canopy isoprene fluxes could allow for a more accurate quantification and for a better understanding of seasonal isoprene flux. Here, we indicate that leaf phenology plays an important role in seasonal variation of isoprene emissions, especially because different leaf ages present different isoprene emission capacity and the proportion of leaf age changes seasonally in Amazonia. However, when air temperature is the highest, isoprene emission could be more stimulated by this factor, even though mature LAI is still not at its maximum. We suggest future research to verify whether tree species that present a regular seasonal leaf flushing are isoprene emitters and the strength of those emissions by leaf age.

4.2. How can a consideration of leaf phenology observed in the field help to improve model estimates of seasonal isoprene emissions?

Modeling of isoprene emissions from the Amazonian rainforest has been carried out for around thirty years. The first models were simplified and parameterized with observations from a few short field campaigns (see Table 1 of Alves et al., 2016). With the increase in available data, more driving forces of isoprene emission were accounted for in the latest versions of models, as the case of the MEGAN 2.1, which has been improved with a multi-layer canopy model that accounts for light interception and leaf

481 temperature within the canopy, and includes changes in emissions due to leaf age that are
482 typically driven by satellite retrievals of LAI development (Guenther et al., 2012).
483 Results presented here are from MEGAN 2.1 estimates with local observations of
484 PAR, air temperature, and satellite-based leaf phenology. Initially, the default MEGAN
485 2.1 simulations did not fully capture the seasonal pattern of observed isoprene emission,
486 with non-significant correlation between model estimates and observations (R^2= 0.16,
487 P>0.05, Table 2). This could be due to the near saturation of LAI seasonality in
488 Amazonian evergreen forests and poor representation of leaf age effect on isoprene
489 emission capacity of tropical tree species in the default MEGAN 2.1. Furthermore, by
490 using the camera-derived LAI phenology and the leaf age demographics to update the
491 leaf age algorithm of the default MEGAN 2.1, we improved estimates of the proportion
492 of leaves in different leaf age categories for the site, but there were a lack of observations
493 for assigning the relative isoprene emission capacity for each age class.
494 It has been suggested that MEGAN uncertainties are mostly related to short-term
495 and long-term seasonality of the isoprene emission capacity (Niinemets et al., 2010). For
496 instance, for an Asian tropical forest, isoprene emission capacity was reported to be four
497 times lower than the default value of the MEGAN model (Langford et al., 2010), whereas
498 aircraft flux measurements in the Amazon were 35% higher than the MEGAN values (Gu
499 et al., 2017); and satellite retrievals suggested significantly lower isoprene emissions (30-
500 40 % in Amazonia and northern Africa) with respect to the MEGAN-MOHYCAN
501 database (Bauwens et al., 2016). These all demonstrate that isoprene emission capacity is
502 not well represented in the model for regions where there are few or no measurements.

503 For a sensitivity test, we parameterized the MEGAN 2.1 leaf age algorithm with
504 observed isoprene emission capacity among different leaf ages of *E. coriacea* (Alves et
505 al., 2014). The resulting simulation showed that by knowing the leaf age class
506 distribution and the isoprene emission capacity for each age class, MEGAN 2.1 estimates
507 can be improved and better agree with observations in terms of seasonal behavior. To
508 date, there is very little information about isoprene emission capacity for different leaf
509 ages of Amazonian plant species (Alves et al., 2014; Kuhn et al., 2004a). The scarcity of
510 observational studies in the field, along with the huge biodiversity and heterogeneity of
511 the Amazonian ecosystems, creates a challenge to optimize the isoprene emission
512 capacity parameterization in MEGAN and other models. Therefore, while introducing
513 local seasonal changes of canopy leaf age fractions in the model should improve
514 estimates, seasonal variations in isoprene emission capacity also need to be characterized
515 to better represent the effects of leaf phenology on tropical ecosystem isoprene emissions.
516
517 **4.3. Possible limitations**
518 This study correlates available data of different scales and approaches. Thus, there
519 are limitations that need to be considered. One is the uncertainty related to the method
520 used to measure ground-based isoprene fluxes. The uncertainties of the REA flux
521 measurements ranged from 27.1% to 44.9% (more details in section 1 of Supplementary
522 Information). However, this study shows the largest dataset of seasonal isoprene fluxes in
523 Amazonia presented to date and results presented here are similar to previous
524 investigations, when the same seasons are compared (see Table 1 of Alves et al., 2016).

525 Another limitation is the uncertainty of MEGAN estimates. It has been shown that
526 models tend to agree with observations within ~30% for canopy scale studies with site-
527 specific parameters (Lamb et al., 1996). Here, part of the low correlation between
528 observations and MEGAN 2.1 estimates is possibly due to short periods of measurements
529 and data gaps. There were data gaps of PAR and temperature for a few months in 2013.
530 This could influence the mean flux obtained from model estimates. Also, REA
531 measurements were carried out in intensive campaigns of six days per month, which may
532 not represent the flux for the entire month. Therefore, the limited data availability is still
533 challenging our understanding of isoprene emission seasonality.
534
535 **5. Summary and Conclusions**
536 To understand the pattern of isoprene seasonal fluxes in Amazonia is a difficult
537 task when considering the important role of Amazonian forests in accounting for global
538 BVOC and very limited field based observations in Amazonia. Seasonal variation of light
539 and temperature are thought to primarily drive isoprene seasonal emissions. However,
540 less notable factors in tropical forests might also influence ecosystem isoprene emission.
541 Here, we suggest that leaf phenology, especially when accounting for the effect of leaf
542 demography (canopy leaf age composition) and leaf ontogeny (age-dependent isoprene
543 emission capacity), has an important effect on seasonal changes of the ecosystem
544 isoprene emissions, which could play even more important role in regulating ecosystem
545 isoprene fluxes than light and temperature at seasonal timescale in tropical forests. To the
546 best of our knowledge, these results are the first to show the importance of leaf
547 phenology on seasonal isoprene emissions in a tropical forest.

548 Albeit there are uncertainties related to measurements and modeling, results
549 presented here suggested that the unknown isoprene emission capacity for the different
550 leaf age classes found in the forest may be the main reason why MEGAN 2.1 did not
551 represent well the observed seasonality of isoprene fluxes. Additionally, part of these
552 model uncertainties arises because of a lack of representations of canopy structure and
553 light interception, including within-canopy variation in leaf functional traits; the leaf
554 phenology within the canopy; the physical processes by which isoprene is transported
555 within and above the forest canopy; chemical reactions that can take place within the
556 canopy; and, the most difficult to assess, emission variation due to the huge biodiversity
557 in Amazonia. Therefore, more detailed measurements of source and sink processes are
558 encouraged to improve our understanding of the seasonality of isoprene emissions in
559 Amazonia, which will improve surface emission models and will subsequently lead to a
560 better predictive vision of atmospheric chemistry, biogeochemical cycles, and climate.
561
562 **6. Data Availability**
563 Even though the data are still not available in any public repository, the data are
564 available upon request from the first author.
565
566 **7. Acknowledgements**
567 The authors thank the National Institute for Amazonian Research (INPA) for continuous
568 support. We acknowledge the support by the Large Program of Biosphere-Atmosphere
569 Interactions (LBA) for the logistics and the micrometeorological group for their
570 collaboration concerning the meteorological parameters. We acknowledge Kolby Jardine
571 for providing the gas standard to calibrate the analytical system, and Paula Regina Corain

572 Lopes for the help in the fieldwork. J.W. is supported by DOE BER funded NGEE-
573 Tropics project (contract # DE- SC00112704) to Brookhaven National Laboratory.

574

575 **8. References**

576 Adams, D. K., Fernandes, R. M. S., Holub, K. L., Gutman, S. I., Barbosa, H. M. J.,
577 Machado, L. A. T., Calheiros, A. J. P., Bennett, R. A., Robert Kursinski, E., Sapucci, L.
578 F., Demets, C., Chagas, G. F. B., Arellano, A., Filizola, N., Rocha, A. A. A., Silva, R. A.,
579 Assunção, L. M. F., Cirino, G. G., Pauliquevis, T., Portela, B. T. T., Sá, A., De Sousa, J.
580 M. and Tanaka, L. M. S.: The Amazon dense GNSS meteorological network: a new
581 approach for examining water vapor and deep convection interactions in the Tropics,
582 Bull. Amer. Meteor. Soc., 96(12), 2151–2165, doi:10.1175/BAMS-D-13-00171.1, 2015.
583
584 Adams, D. K., Fernandes, R. M. S. and Maia, J. M. F.: GNSS Precipitable Water Vapor
585 from an Amazonian Rain Forest Flux Tower, J. Atmos. Ocean. Technol., 28(10), 1192–
586 1198, doi:10.1175/JTECH-D-11-00082.1, 2011.
587
588 Adams, D. K., Gutman, S. I., Holub, K. L. and Pereira, D. S.: GNSS observations of deep
589 convective time scales in the Amazon, Geophys. Res. Lett., 40(11), 2818–2823, 2013.
590
591 Alves, E. G., Harley, P., Gonçalves, J. F. C., Moura, C. E. S. and Jardine, K.: Effects of
592 light and temperature on isoprene emission at different leaf developmental stages of
593 eschweilera coriacea in central amazon, Acta Amaz., 44(1), 9–18, doi:10.1590/S0044-
594 59672014000100002, 2014.
595
596 Alves, E. G., Jardine, K., Tota, J., Jardine, A., Yãnez-Serrano, A. M., Karl, T., Tavares,
597 J., Nelson, B., Gu, D., Stavrakou, T., Martin, S., Artaxo, P., Manzi, A. and Guenther, A.:
598 Seasonality of isoprenoid emissions from a primary rainforest in central Amazonia,
599 Atmos. Chem. Phys., 16(6), 3903–3925, doi:10.5194/acp-16-3903-2016, 2016.
600
601 Andreae, M. O., Artaxo, P., Brandão, C., Carswell, F. E., Ciccioli, P., Da Costa, a. L.,
602 Gulf, a. D., Esteves, J. L., Gash, J. H. C., Grace, J., Kabat, P., Lelieveld, J., Malhi, Y.,
603 Manzi, a. O., Meixner, F. X., Nobre, a. D., Nobre, C., Ruivo, M. D. L. P., Silva-Dias,
604 M. a., Stefani, P., Valentini, R., Von Jouanne, J. and Waterloo, M. J.: Biogeochemical
605 cycling of carbon, water, energy, trace gases, and aerosols in Amazonia: The LBA-
606 EUSTACH experiments, J. Geophys. Res. D Atmos., 107(20),
607 doi:10.1029/2001JD000524, 2002.
608
609 Arneth, A., Monson, R. K., Schurgers, G., Niinemets, U. and Palmer, P. I.: Why are
610 estimates of global terrestrial isoprene emissions so similar (and why is this not so for
611 monoterpenes)? Atmos. Chem. Phys., 8(16), 4605–4620, doi:10.5194/acp-8-4605-2008,
612 2008.
613

614 Artaxo, P., Rizzo, L. V, Brito, J. F., Barbosa, H. M. J., Arana, A., Sena, E. T., Cirino, G.
615 G., Bastos, W., Martin, S. T. and Andreae, M. O.: Atmospheric aerosols in Amazonia and
616 land use change: from natural biogenic to biomass burning conditions, Faraday Discuss.,
617 165, 203, doi:10.1039/c3fd00052d, 2013.
618
619 Barkley, M. P., Palmer, P. I., Kuhn, U., Kesselmeier, J., Chance, K., Kurosu, T. P.,
620 Martin, R. V., Helmig, D. and Guenther, A.: Net ecosystem fluxes of isoprene over
621 tropical South America inferred from Global Ozone Monitoring Experiment (GOME)
622 observations of HCHO columns, J. Geophys. Res., 113(D20), D20304,
623 doi:10.1029/2008JD009863, 2008.
624
625 Barkley, M. P., Palmer, P. I., De Smedt, I., Karl, T., Guenther, A. and Van Roozendael,
626 M.: Regulated large-scale annual shutdown of Amazonian isoprene emissions? Geophys.
627 Res. Lett., 36(4), L04803, doi:10.1029/2008GL036843, 2009.
628
629 Barkley, M. P., Smedt, I. De, Van Roozendael, M., Kurosu, T. P., Chance, K., Arneth, A.,
630 Hagberg, D., Guenther, A., Paulot, F., Marais, E. and Mao, J.: Top-down isoprene
631 emissions over tropical South America inferred from SCIAMACHY and OMI
632 formaldehyde columns, J. Geophys. Res. Atmos., 118(12), 6849–6868,
633 doi:10.1002/jgrd.50552, 2013.
634
635 Bauwens, M., Stavrakou, T., Müller, J. F., De Smedt, I., Van Roozendael, M., van der
636 Werf, G. R., Wiedinmyer, C., Kaiser, J. W., Sindelarova, K. and Guenther, A.: Nine
637 years of global hydrocarbon emissions based on source inversion of OMI formaldehyde
638 observations, Atmos. Chem. Phys., 16(15), 10133–10158, doi:10.5194/acp-16-10133-
639 2016, 2016.
640
641 Bauwens, M., Stavrakou, T., Müller, J.-F., Van Schaeybroeck, B., De Cruz, L., De Troch,
642 R., Giot, O., Hamdi, R., Termonia, P., Laffineur, Q., Amelynck, C., Schoon, N.,
643 Heinesch, B., Holst, T., Arneth, A., Ceulemans, R., Sanchez-Lorenzo, A., and Guenther,
644 A.: Recent past (1979–2014) and future (2070–2099) isoprene fluxes over Europe
645 simulated with the MEGAN-MOHYCAN model, Biogeosciences Discuss.,
646 https://doi.org/10.5194/bg-2017-532, in review, 2017.
647
648 Bowling, D. R., Turnipseed, A. A., Delany, A. C., Baldocchi, D. D., Greenberg, J. P.
649 and Monson, R. K.: The use of relaxed eddy accumulation to measure biosphere-
650 atmosphere exchange of isoprene and other biological trace gases, Oecologia, 116(3),
651 306–315, doi:10.1007/s004420050592, 1998.
652
653 Brilli, F., Gioli, B., Fares, S., Terenzio, Z., Zona, D., Gielen, B., Loreto, F., Janssens, I.
654 A. and Ceulemans, R.: Rapid leaf development drives the seasonal pattern of volatile
655 organic compound (VOC) fluxes in a “coppiced” bioenergy poplar plantation, Plant, Cell
656 Environ., 39(3), 539–555, doi:10.1111/pce.12638, 2016.
657
658 Claeys, M., Graham, B., Vas, G., Wang, W., Vermeylen, R., Pashynska, V., Cafmeyer, J.,
659 Maenhaut, W., Guyon, P., Andreae, M. O. and Artaxo, P.: Formation of secondary

organic aerosols through photooxidation of isoprene, Science, 303(5661), 1173–1176, doi:10.1126/science.1092805, 2004.

Cuartas, L. A., Tomasella, J., Nobre, A. D., Nobre, C. A., Hodnett, M. G., Waterloo, M. J., Oliveira, S. M. De, Randow, R. D. C. Von, Trancoso, R. and Ferreira, M.: Distributed hydrological modeling of a micro-scale rainforest watershed in Amazonia: Model evaluation and advances in calibration using the new HAND terrain model, J. Hydrol., 462–463, 15–27, doi:10.1016/j.jhydrol.2011.12.047, 2012.

de Araújo, A. C., Dolman, A. J., Waterloo, M. J., Gash, J. H. C., Kruijt, B., Zanchi, F. B., de Lange, J. M. E., Stoevelaar, R., Manzi, A. O. and Nobre, A. D.: The spatial variability of CO2 storage and the interpretation of eddy covariance fluxes in central Amazonia, Agric. For. Meteorol., 150(2), 226–237, doi:10.1016/j.agrformet.2009.11.005, 2010.

Delwiche, C. F. and Sharkey, T. D.: Rapid appearance of 13C in biogenic isoprene when 13CO2 is fed to intact leaves, Plant. Cell Environ., 16(5), 587–591, doi:10.1111/j.1365-3040.1993.tb00907.x, 1993.

Goldstein, A. H. and Galbally, I. E.: Known and Unexplored Organic Constituents in the Earth's Atmosphere, Environ. Sci. Technol., 41(5), 1514–1521, doi:10.1021/es072476p, 2007.

Gu, D., Guenther, A. B., Shilling, J. E., Yu, H., Huang, M., Zhao, C., Yang, Q., Martin, S. T., Artaxo, P., Kim, S., Seco, R., Stavrakou, T., Longo, K. M., Tóta, J., de Souza, R. A. F., Vega, O., Liu, Y., Shrivastava, M., Alves, E. G., Santos, F. C., Leng, G. and Hu, Z.: Airborne observations reveal elevational gradient in tropical forest isoprene emissions, Nat. Commun., 8-, 15541, doi:10.1038/ncomms15541, 2017.

Guenther, A.: The contribution of reactive carbon emissions from vegetation to the carbon balance of terrestrial ecosystems., Chemosphere, 49(8), 837–44, 2002.

Guenther, A. B., Jiang, X., Heald, C. L., Sakulyanontvittaya, T., Duhl, T., Emmons, L. K. and Wang, X.: The Model of Emissions of Gases and Aerosols from Nature version 2.1 (MEGAN2.1): an extended and updated framework for modeling biogenic emissions, Geosci. Model Dev., 5(2), 1503–1560, doi:10.5194/gmdd-5-1503-2012, 2012.

Guenther, A., Karl, T., Harley, P., Wiedinmyer, C., Palmer, P. I. and Geron, C.: Estimates of global terrestrial isoprene emissions using MEGAN (Model of Emissions of Gases and Aerosols from Nature), Atmos. Chem. Phys., 6(1), 3181–3210, doi:10.5194/acpd-6-107-2006, 2006.

Harley, P., Monson, R. and Lerdau, M.: Ecological and evolutionary aspects of isoprene emission from plants, Oecologia, 118, 109–123, 1999.

Harley, P., Vasconcellos, P., Vierling, L., Pinheiro, C. C. D. S., Greenberg, J., Guenther, A., Klinger, L., Almeida, S. S. De, Neill, D., Baker, T., Phillips, O., Malhi, Y. and De Almeida, S. S.: Variation in potential for isoprene emissions among Neotropical forest sites, Glob. Chang. Biol., 10(5), 630–650, doi:10.1111/j.1529-8817.2003.00760.x, 2004.

Huete, A. R., Didan, K., Shimabukuro, Y. E., Ratana, P., Saleska, S. R., Hutyra, L. R., Yang, W., Nemani, R. R. and Myneni, R.: Amazon rainforests green-up with sunlight in dry season, Geophys. Res. Lett., 33, 2–5, doi:10.1029/2005GL025583, 2006.

Jardine, K., Chambers, J., Alves, E. G., Teixeira, A., Garcia, S., Holm, J., Higuchi, N., Manzi, A., Abrell, L., Fuentes, J. D., Nielsen, L. K., Torn, M. S. and Vickers, C. E.: Dynamic balancing of isoprene carbon sources reflects photosynthetic and photorespiratory responses to temperature stress, Plant Physiol., 166(4), 2051–2064, doi:10.1104/pp.114.247494, 2014.

Kesselmeier, J., Ciccioli, P., Kuhn, U., Stefani, P., Biesenthal, T., Rottenberger, S., Wolf, A., Vitullo, M., Valentini, R., Nobre, A., Kabat, P. and Andreae, M. O.: Volatile organic compound emissions in relation to plant carbon fixation and the terrestrial carbon budget, Global Biogeochem. Cycles, 16(4), 73-1-73–9, doi:10.1029/2001GB001813, 2002.

Kuhn, U., Rottenberger, S., Biesenthal, T., Wolf, A., Schebeske, G., Ciccioli, P., Brancaleoni, E., Frattoni, M., Tavares, T. M. and Kesselmeier, J.: Isoprene and monoterpene emissions of Amazonian tree species during the wet season: Direct and indirect investigations on controlling environmental functions, J. Geophys. Res., 107(D20), 8071, doi:8071 10.1029/2001jd000978, 2002.

Kuhn, U., Rottenberger, S., Biesenthal, T., Wolf, A., Schebeske, G., Ciccioli, P. and Kesselmeier, J.: Strong correlation between isoprene emission and gross photosynthetic capacity during leaf phenology of the tropical tree species Hymenaea courbaril with fundamental changes in volatile organic compounds emission composition during early leaf development, Plant, Cell Environ., 27(12), 1469–1485, doi:10.1111/j.1365-3040.2004.01252.x, 2004a.

Kuhn, U., Rottenberger, S., Biesenthal, T., Wolf, a., Schebeske, G., Ciccioli, P., Brancaleoni, E., Frattoni, M., Tavares, T. M. and Kesselmeier, J.: Seasonal differences in isoprene and light-dependent monoterpene emission by Amazonian tree species, Glob. Chang. Biol., 10(5), 663–682, doi:10.1111/j.1529-8817.2003.00771.x, 2004b.

Kuzma, J. and Fall, R.: Leaf Isoprene Emission Rate Is Dependent on Leaf Development and the Level of Isoprene Synthase., Plant Physiol., 101(2), 435–440, 1993.

Lamb, B., Pierce, T., Baldocchi, D., Allwine, E., Dilts, S., Westberg, H., Geron, C., Guenther, A., Klinger, L., Harley, P. and Zimmerman, P.: Evaluation of forest canopy models for estimating isoprene emissions, J. Geophys. Res., 101(D17), 22787–22797, doi:10.1029/96JD00056, 1996.

751 Langford, B., Misztal, P. K., Nemitz, E., Davison, B., Helfter, C., Pugh, T. A. M.,
752 MacKenzie, A. R., Lim, S. F. and Hewitt, C. N.: Fluxes and concentrations of volatile
753 organic compounds from a South-East Asian tropical rainforest, Atmos. Chem. Phys.,
754 10(17), 8391–8412, doi:10.5194/acp-10-8391-2010, 2010.
755
756 Lichtenthaler, H. K., Rohmer, M. and Schwender, J.: Two independent biochemical
757 pathways for isopentenyl diphosphate and isoprenoid biosynthesis in higher plants,
758 Physiol. Plant., 101(3), 643–652, doi:10.1111/j.1399-3054.1997.tb01049.x, 1997.
759
760 Lopes, A. P., Nelson, B. W., Wu, J., Graça, P. M. L. de A., Tavares, J. V., Prohaska, N.,
761 Martins, G. A. and Saleska, S. R.: Leaf flush drives dry season green-up of the Central
762 Amazon, Remote Sens. Environ., 182, 90–98, doi:10.1016/j.rse.2016.05.009, 2016.
763
764 Loreto, F. and Delfine, S.: Emission of Isoprene from Salt-stressed Eucalyptus globulus
765 Leaves., Plant Physiol., 123(4), 1605–1610, doi:10.1104/pp.123.4.1605, 2000.
766
767 Loreto, F. and Sharkey, T. D.: On the relationship between isoprene emission and
768 photosynthetic metabolites under different environmental conditions, Planta, 189(3),
769 420–424, doi:10.1007/BF00194440, 1993.
770
771 Machado, L. A. T., Laurent, H., Dessay, N. and Miranda, I.: Seasonal and diurnal
772 variability of convection over the Amazonia: A comparison of different vegetation types
773 and large scale forcing, Theor. Appl. Climatol., 78(1–3), 61–77, doi:10.1007/s00704-
774 004-0044-9, 2004.
775
776 Mayrhofer, S., Teuber, M., Zimmer, I., Louis, S., Fischbach, R. J. and Schnitzler, J.-P.:
777 Diurnal and seasonal variation of isoprene biosynthesis-related genes in grey poplar
778 leaves., Plant Physiol., 139(1), 474–484, doi:10.1104/pp.105.066373, 2005.
779
780 Monson, R. K., Harley, P. C., Litvak, M. E., Wildermuth, M., Guenther, A. B.,
781 Zimmerman, P. R. and Fall, R.: Environmental and developmental controls over the
782 seasonal pattern of isoprene emission from aspen leaves, Oecologia, 99(3–4), 260–270,
783 doi:10.1007/BF00627738, 1994.
784
785 Morton, D. C., Nagol, J., Carabajal, C. C., Rosette, J., Palace, M., Cook, B. D., Vermote,
786 E. F., Harding, D. J. and North, P. R. J.: Amazon forests maintain consistent canopy
787 structure and greenness during the dry season, Nature, 506(7487), 221–4,
788 doi:10.1038/nature13006, 2014.
789
790 Myneni, R. B., Yang, W., Nemani, R. R., Huete, A. R., Dickinson, R. E., Knyazikhin, Y.,
791 Didan, K., Fu, R., Negrón Juárez, R. I., Saatchi, S. S., Hashimoto, H., Ichii, K.,
792 Shabanov, N. V, Tan, B., Ratana, P., Privette, J. L., Morisette, J. T., Vermote, E. F., Roy,
793 D. P., Wolfe, R. E., Friedl, M. A., Running, S. W., Votava, P., El-Saleous, N., Devadiga,
794 S., Su, Y. and Salomonson, V. V: Large seasonal swings in leaf area of Amazon
795 rainforests, Proc. Natl. Acad. Sci. U. S. A., 104(12), 4820–4823,
796 doi:10.1073/pnas.0611338104, 2007.

Myneni, R.: MCD15A2H MODIS/Terra+Aqua Leaf Area Index/FPAR 8-day L4 Global 500m SIN Grid V006. ***NASA*** *EOSDIS Land Processes DAAC,* https://doi.org/10.5067/modis/mcd15a2h.006, 2015.

Nelson, B., Tavares, J. V., Wu, J., Lopes, A. P., Marostica, S., Martins, G., Prohaska, N., Albert, L. P., de Araújo, A. C., Manzi, A. O., Saleska, S., Huete, A.: Seasonality of central Amazon Forest Leaf Flush using tower mounted RGB Camera. AGU Fall Meeting, San Francisco, California, 15–19 December 2014, B11G-0107, 2014.

Niinemets, U., Arneth, A., Kuhn, U., Monson, R. K., Penuelas, J. and Staudt, M.: The emission factor of volatile isoprenoids: stress, acclimation, and developmental responses, Biogeosciences, 7(7), 2203–2223, doi:10.5194/bg-7-2203-2010, 2010.

Niinemets, U., Loreto, F. and Reichstein, M.: Physiological and physicochemical controls on foliar volatile organic compound emissions., Trends Plant Sci., 9(4), 180–6, doi:10.1016/j.tplants.2004.02.006, 2004.

Rennó, C. D., Nobre, A. D., Cuartas, L. A., Soares, J. V., Hodnett, M. G., Tomasella, J. and Waterloo, M. J.: HAND, a new terrain descriptor using SRTM-DEM: Mapping terra-firme rainforest environments in Amazonia, Remote Sens. Environ., 112(9), 3469–3481, doi:10.1016/j.rse.2008.03.018, 2008.

Rohmer, M.: From molecular fossils of bacterial hopanoids to the formation of isoprene units: Discovery and elucidation of the methylerythritol phosphate pathway, Lipids, 43(12), 1095–1107, doi:10.1007/s11745-008-3261-7, 2008.

Saleska, S. R., Wu, J., Guan, K., Araujo, A. C., Huete, A., Nobre, A. D. and Restrepo-Coupe, N.: Dry-season greening of Amazon forests, Nature, 531(7594), doi:10.1038/nature16457, 2016.

Samanta, A., Ganguly, S., Hashimoto, H., Devadiga, S., Vermote, E., Knyazikhin, Y., Nemani, R. R. and Myneni, R. B.: Amazon forests did not green-up during the 2005 drought, Geophys. Res. Lett., 37(5), 1–5, doi:10.1029/2009GL042154, 2010.

Schnitzler, J.-P., Lehning, A. and Steinbrecher, R.: Seasonal Pattern of Isoprene Synthase Activity in Quercus robur Leaves and its Significance or Modeling Isoprene Emission Rates, Bot. Acta, 110, 240–243, 1997.

Schwender, J., Zeidler, J., Gröner, R., Müller, C., Focke, M., Braun, S., Lichtenthaler, F. W. and Lichtenthaler, H. K.: Incorporation of 1-deoxy-D-xylulose into isoprene and phytol by higher plants and algae, FEBS Lett., 414(1), 129–134, doi:10.1016/S0014-5793(97)01002-8, 1997.

Stavrakou, T., Müller, J.-F., Bauwens, M., De Smedt, I., Van Roozendael, M., Guenther, A., Wild, M. and Xia, X.: Isoprene emissions over Asia 1979–2012: impact of climate

and land-use changes, Atmos. Chem. Phys., 14(9), 4587–4605, doi:10.5194/acp-14-4587-2014, 2014.

Stavrakou, T., Müller, J.-F., Bauwens, M., De Smedt, I., Van Roozendael, M., De Mazière, M., Vigouroux, C., Hendrick, F., George, M., Clerbaux, C., Coheur, P.-F. and Guenther, A.: How consistent are top-down hydrocarbon emissions based on formaldehyde observations from GOME-2 and OMI? Atmos. Chem. Phys., 15(20), 11861–11884, doi:10.5194/acp-15-11861-2015, 2015.

Stavrakou, T., Müller, J.-F., De Smedt, I., Van Roozendael, M., van der Werf, G. R., Giglio, L. and Guenther, A.: Global emissions of non-methane hydrocarbons deduced from SCIAMACHY formaldehyde columns through 2003–2006, Atmos. Chem. Phys., 9, 3663-3679, https://doi.org/10.5194/acp-9-3663-2009, 2009.

Tóta, J., Fitzjarrald, D. R. and da Silva Dias, M. A. F.: Amazon rainforest exchange of carbon and subcanopy air flow: Manaus LBA site – a complex terrain condition, Scientific World Journal., 2012, 165067, doi:10.1100/2012/165067, 2012.

Wagner, F. H., Hérault, B., Rossi, V., Hilker, T., Maeda, E. E., Sanchez, A., Lyapustin, A. I., Galvão, L. S., Wang, Y. and Aragão, L. E. O. C.: Climate drivers of the Amazon forest greening, PLoS One, 12(7), 1–15, doi:10.1371/journal.pone.0180932, 2017.

Wu, J., Albert, L. P., Lopes, A. P., Restrepo-Coupe, N., Hayek, M., Wiedemann, K. T., Guan, K., Stark, S. C., Christoffersen, B., Prohaska, N., Tavares, J. V., Marostica, S., Kobayashi, H., Ferreira, M. L., Campos, K. S., Silva, R. da, Brando, P. M., Dye, D. G., Huxman, T. E., Huete, A. R., Nelson, B. W. and Saleska, S. R.: Leaf development and demography explain photosynthetic seasonality in Amazon evergreen forests, Science, 351(6276), doi:10.1126/science.aad5068, 2016.

Yáñez-Serrano, A. M., Nölscher, a C., Williams, J., Wolff, S., Alves, E., Martins, G. a, Bourtsoukidis, E., Brito, J., Jardine, K. J., Artaxo, P. and Kesselmeier, J.: Diel and seasonal changes of biogenic volatile organic compounds within and above an Amazonian rainforest, Atmos. Chem. Phys., 15, 3359–3378, doi:10.5194/acp-15-3359-2015, 2015.

Tables

Table 1: Environmental and biological factors used to input the MEGAN 2.1: number of days with data available for each variable for the year 2013

	Jan	Feb	Mar	Apr	May	Jun	Jul	Aug	Sep	Oct	Nov	Dec
PAR	*n*=31	*n*=28	*n*=31	*n*=30	*n*=31	*n*=30	*n*=31	*n*=15	*n*=30	*n*=18	*n*=19	*n*=15
Air temperature	*n*=31	*n*=28	*n*=31	*n*=30	*n*=31	*n*=30	*n*=31	*n*=15	*n*=30	*n*=18	*n*=19	*n*=15
CAMERA-LAI*	*n*=5	*n*=4	*n*=5	*n*=5	*n*=5	*n*=5	*n*=5	*n*=5	*n*=5	*n*=5	*n*=5	*n*=5
MODIS-LAI**	*n*=4	*n*=4	*n*=4	*n*=3	*n*=5	*n*=4	*n*=4	*n*=4	*n*=4	*n*=3	*n*=4	*n*=4

* Number of days with images analyzed to derive CAMERA-LAI as described in section 2.4.
** Number of days that the satellite passed over the site domain.

Table 2: Correlation coefficient, R^2, of regressions for ground-based isoprene flux, satellite-derived isoprene flux, environmental factors, biological factors, and MEGAN 2.1 simulations

	Ground-based isoprene flux	Satellite-derived isoprene flux (2013 year)
PAR	0.007[a]	0.55[c]
PAR – REA measurement days	0.11[a]	-----
Air temperature	0.15[a]	0.79[c]
Air temperature – REA measurement days	0.39[a]	-----
young LAI	0.04[a]	0.35[b]
mature LAI	0.59[b]	0.05[a]
old LAI	-0.6[b]	-0.4[b]
Photosynthetic capacity*	0.49[a]	-----
GPP*	0.36[a]	-----
MEGAN (MODIS-LAI)	0.16[a]	0.76[c]
MEGAN (CAMERA-LAI)	0.11[a]	0.67[c]
MEGAN (MODIS-LAI) EAF changed	0.19[a]	0.66[c]
MEGAN (CAMERA-LAI) EAF changed	0.52[b]	0.59[c]
Ground-based isoprene flux	-----	0.13[a]

PAR, photosynthetic active radiation; GPP, gross primary productivity;
EAF, emission activity factor;
* Data from Wu *et al.* (2016)
[a] not statistically significant ($P > 0.05$)

[b] statistically significant ($P < 0.05$)
[c] statistically significant ($P < 0.001$)

Figure captions

Figure 1. Location of the experimental site in central Amazonia – K34 tower. Hill-shaded digital elevation data used as background topography is from the Shuttle Radar Topography Mission, with resolutions of ~900m (top panel) and ~30m (lower panel). White ring indicates two km radius around the flux tower. Elevation scale for lower panel is "meters above sea level".

Figure 2. (a) Monthly averages of photosynthetic active radiation (PAR) and (b) air temperature from 2005 to 2013 at the K34 tower site (measured every 30 min during 6:00-18:00h, local time). (c) OMI satellite-derived isoprene flux in a resolution of 0.5º centered on K34 tower site from 2005 to 2013. Monthly averages of isoprene flux were scaled to 10:00-14:00, local time. Error bars represent one standard error of the mean.

Figure 3. (a) Monthly cumulative precipitation given by the Tropical Rainfall Measuring Mission (TRMM) for the K34 tower domain in 2013. (b) Monthly averages of PAR and (c) air temperature, both measured every 30 minutes during 6:00-18:00h, local time, at the K34 tower site in 2013. (d) Isoprene flux measured with the REA system at the K34 tower site in 2013; and OMI satellite-derived isoprene flux for the K34 tower region.

Figure 4. CAMERA-LAI derived for the K34 tower site. CAMERA-LAI data are presented in three different leaf age classes: young LAI, mature LAI and old LAI. Error bars represent one standard deviation from the mean. Background color shadings indicate each season and are explicit in the legend. DWT season and WDT season stand for the dry-to-wet transition season and the wet-to-dry transition season, respectively.

Figure 5: Isoprene flux observed (REA) and estimated with MEGAN 2.1 default mode, leaf age algorithm driven by MODIS-LAI, and with MEGAN 2.1 leaf age algorithm driven by CAMERA-LAI. EAF stands for emission activity factor, which was changed for the different leaf age classes based on emissions of *E. coriacea* (Alves et al., 2014).

Figure 6. (a) Emission activity factor (EAF) of isoprene for each leaf age class assigned in the default mode of MEGAN 2.1 proportional to leaf age class distribution derived from field observations (CAMERA-LAI). (b) Isoprene EAF for each leaf age class, obtained from leaf level measurements of the tree species *E. coriacea,* proportional to leaf age class distribution derived from field observations (CAMERA-LAI). Observations of the tree species *E. coriacea* (Alves *et al*., 2014) and CAMERA-LAI are both from the K34 site.

Figures

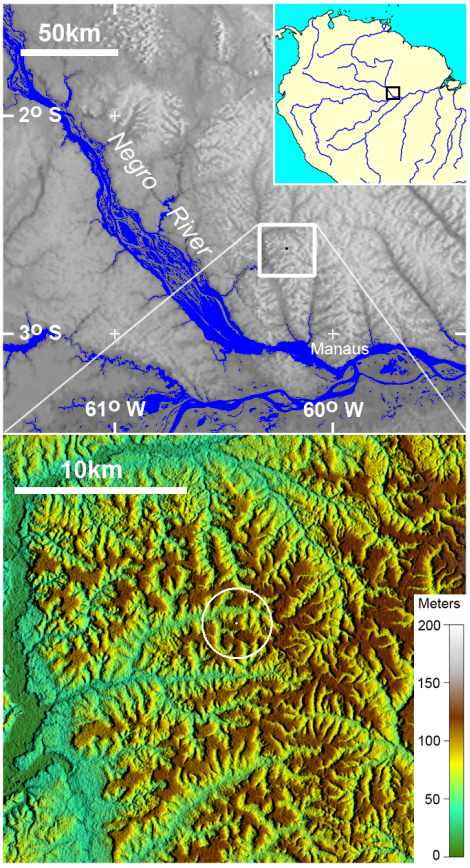

Figure 1. Location of the experimental site in central Amazonia – K34 tower. Hill-shaded digital elevation data used as background topography is from the Shuttle Radar Topography Mission, with resolutions of ~900m (top panel) and ~30m (lower panel). White ring indicates two km radius around the flux tower. Elevation scale for lower panel is "meters above sea level".

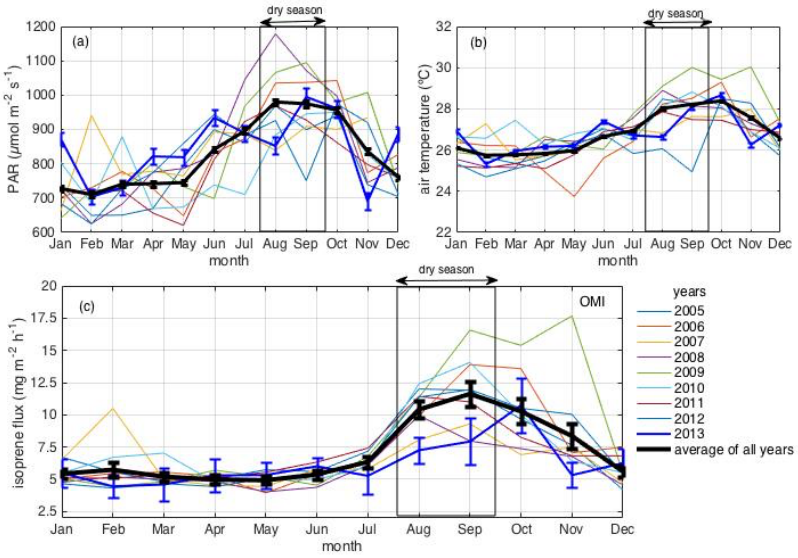

951

952 **Figure 2**. (a) Monthly averages of photosynthetic active radiation (PAR) and (b) air
953 temperature from 2005 to 2013 at the K34 tower site (measured every 30 min during -
954 6:00-18:00h, local time). (c) OMI satellite-derived isoprene flux in a resolution of 0.5º
955 centered on K34 tower site from 2005 to 2013. Monthly averages of isoprene flux were
956 scaled to 10:00-14:00, local time. Error bars represent one standard error of the mean.

957

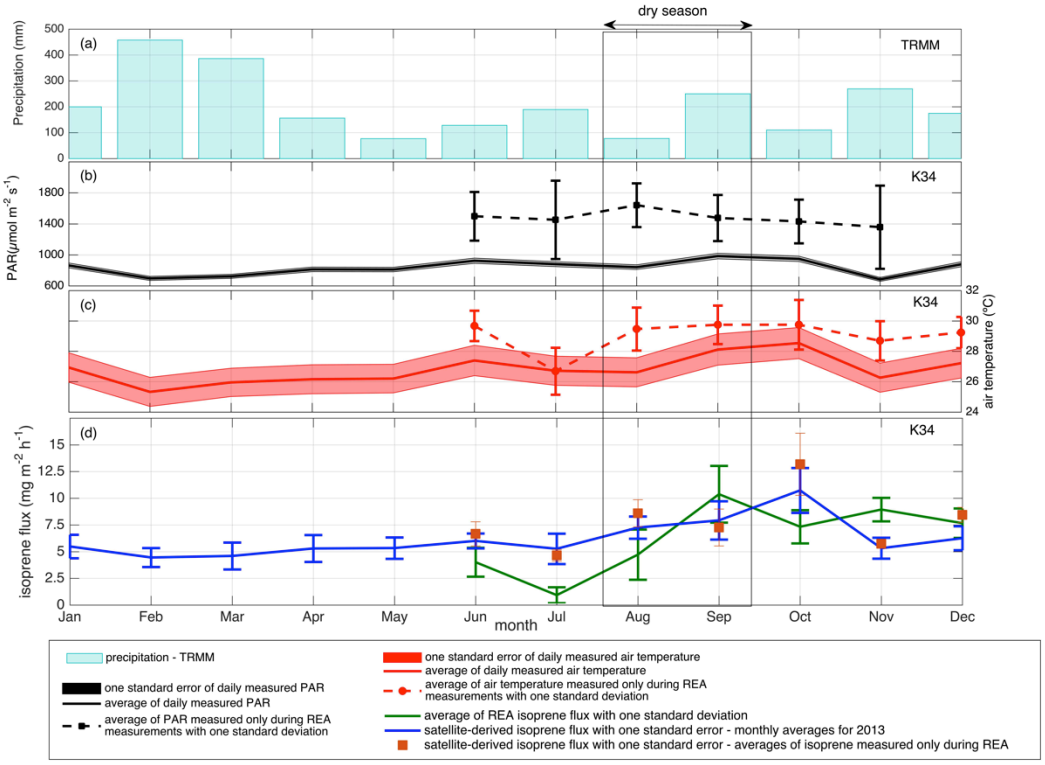

958

959 **Figure 3**. (a) Monthly cumulative precipitation given by the Tropical Rainfall Measuring
960 Mission (TRMM) for the K34 tower domain in 2013. (b) Monthly averages of PAR and
961 (c) air temperature, both measured every 30 minutes during 6:00-18:00h, local time, at
962 the K34 tower site in 2013. (d) Isoprene flux measured with the REA system at the K34
963 tower site in 2013; and OMI satellite-derived isoprene flux for the K34 tower region.

964

965

966

967

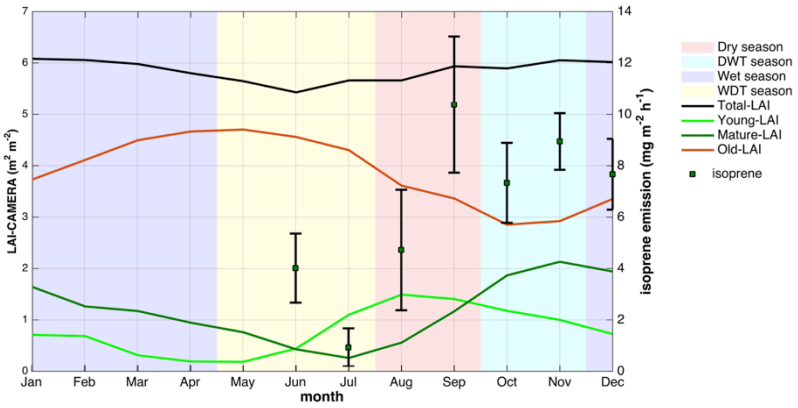

968

969 **Figure 4.** CAMERA-LAI derived for the K34 tower site. CAMERA-LAI data are
970 presented in three different leaf age classes: young LAI, mature LAI and old LAI. Error
971 bars represent one standard deviation from the mean. Background color shadings indicate
972 each season and are explicit in the legend. DWT season and WDT season stand for the
973 dry-to-wet transition season and the wet-to-dry transition season, respectively.

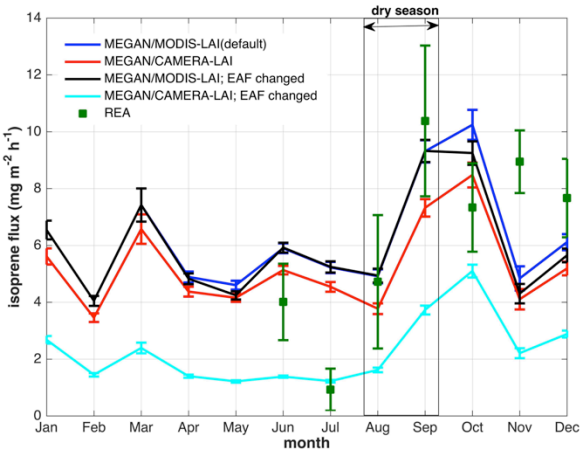

974

975 **Figure 5**: Isoprene flux observed (REA) and estimated with MEGAN 2.1 default mode,
976 leaf age algorithm driven by MODIS-LAI, and with MEGAN 2.1 leaf age algorithm
977 driven by CAMERA-LAI. EAF stands for emission activity factor, which was changed
978 for the different leaf age classes based on emissions of *E. coriacea* (Alves et al., 2014).

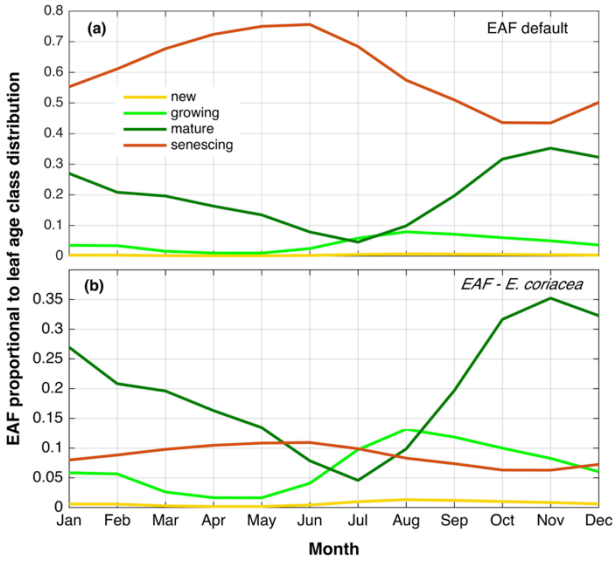

Figure 6. (a) Emission activity factor (EAF) of isoprene for each leaf age class assigned in the default mode of MEGAN 2.1 proportional to leaf age class distribution derived from field observations (CAMERA-LAI). (b) Isoprene EAF for each leaf age class, obtained from leaf level measurements of the tree species *E. coriacea,* proportional to leaf age class distribution derived from field observations (CAMERA-LAI). Observations of the tree species *E. coriacea* (Alves *et al*., 2014) and CAMERA-LAI are both from the K34 site.